

## CHAPTER 3

### Materials and methods

This chapter proposed the materials and methods which use in this study. The number of samples was calculated with two dependence mean formula. The methods were divided into two phases following as the research objective. The first phase was quantified the accuracy of DIR on MVCT by the eight methods which assessed in phantom and nasopharyngeal cases for known and unknown offset investigation. The DIR accuracy on kVCT images were used to compare and the validation in terms of intensity-based, volume-based and deformation field analysis were used to evaluate the accuracy. For the second phase, the impact of DIR methods on dose accumulation was evaluated by using the 1<sup>st</sup> day MVCT and weekly MVCT images of five NPC patients. The weekly registration accuracy and the cumulative dose deviations from the initial treatment plan were analyzed, and correlations of these variables with the accuracy of DIR were explored.

#### 3.1 Sample size calculation

The two dependence mean is used to compare the means of two sets of scores that are directly related to each other as in equation 3.1. For the raw data (Monica *et al.*, 2013), the head and neck patient images performed by two DIR methods for evaluating the accuracy. The difference of mean value between two methods were 0.0095. The standard deviation of mean difference was 0.0061. Therefore, the number of samples which use in this study at least five case set. Following to the two dependence mean formula for calculating the sample size of the study is

$$n = \frac{2\sigma^2(Z_{\alpha/2} + Z_{\beta})^2}{\Delta^2} \quad (3.1)$$

Where  $n$  = number of sample

$\sigma$  = standard deviation of mean difference = 0.0061

Delta = difference of mean value = 0.0095

Alpha = 0.05,  $Z_{\alpha/2}$  = 1.959964

Beta = 0.10,  $Z_{\beta}$  = 1.281552

### 3.2 Phase I: DIR accuracy on MVCT images quantification

#### 3.2.1 Phantoms and patients

Regarding the first research objective, to quantify the accuracy of deformable image registration on MVCT images by various DIR methods, the DIR accuracy on kVCT images were used to compare, the investigation was divided into two groups: phantom studies and clinical studies.

The phantom studies were designed to investigate DIR accuracy in terms of known offsets investigation. In the clinical studies, the MVCT images from five nasopharyngeal carcinoma patients were randomly selected for carrying out the unknown offset investigation.

##### 1) Known offset investigation

A total of twelve shapes in the source and the target images were obtained by using acrylic materials (density 1.15 g/cm<sup>3</sup>) and tissue equivalent materials (diethylhexyl phthalate: DEHP, density 1.02 g/cm<sup>3</sup>) inserted in cubic phantom to simulate the rigid and non-rigid volume changes.

##### 1.1) Rigid volume changes;

As regards the rigid volume changes, the in-house acrylic phantom in various sizes and shapes as in Figure 3.1(b) were used to simulate the rigid

volume change of the target and organ at risk (OAR) with its known offset values. Regarding the areas of deformation, the tissue/air interface and the tissue/tissue interface were used to assess as in Figure 3.1 (c).

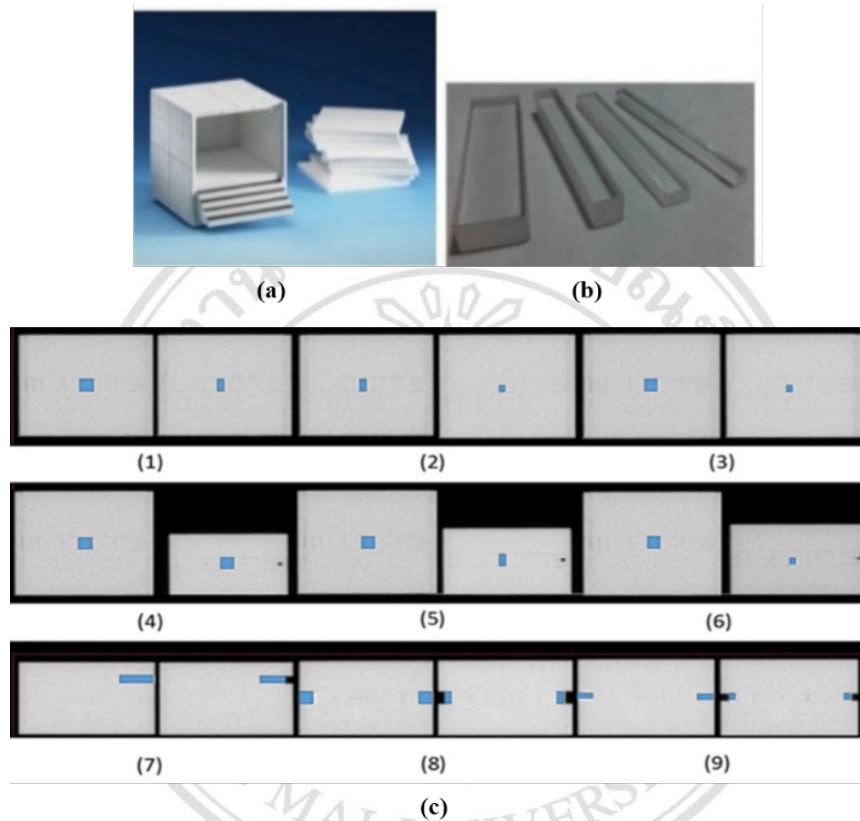


Figure 3.1 (a) Cubic phantom (source: <http://www.dosepoint.de/products/veriqa/easy-cube.html>) (b) In-house acrylic material sets to simulate the rigid volume changes, and (c) A nine shapes in the source and the target images were obtained by using acrylic materials to investigate in tissue/air interface and the tissue/tissue interface.

Regarding the rigid-volume change studies, the width of original acrylic varied with 3 and 2.0 cm and reduced to 1.0 cm (Varadhan *et al.*, 2013) in lateral and vertical direction for tissue/tissue interface as phantom no. 1-3 in Figure 3.1(c) and reduced by 1.0 cm combined 3 cm translation (Castelli *et al.*, 2015) in vertical direction as phantom no. 4-6 in Figure 3.1(c). The tissue/air interface areas were also investigated as phantom no. 7-9 in Figure 3.1(c).

## 1.2) Non-Rigid volume changes;

As regards the non-rigid volume changes, the superflab synthetic gel, diethylhexyl phthalate: DEHP tissue-equivalence material in the bent, curved, and pressed shapes as in Figure 3.2(a) were inserted in the cubic phantom to simulate the non-rigid volume changes. The simulation mimics the relationship between bony anatomy, which is non-deformable and soft-tissue, which is deformable as in Figure 3.2(b).

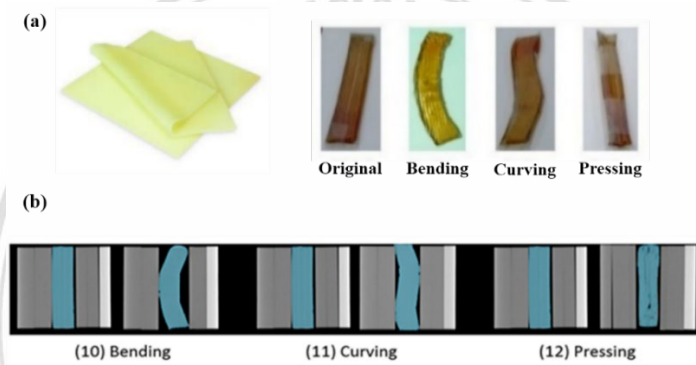


Figure 3.2 (a) the superflab synthetic gel, DEHP with a different shape to investigate the non-rigid volume change (source: <http://www.bebig.com>), and (b) The three shapes in the source and the target images were obtained by using tissue equivalent materials in bent (no.10), curved(no.11) and pressed shape (no.12) for non-rigid investigation.

## 2) Unknown offset investigation

Regarding the unknown offset investigation in clinical cases, this study has institutional ethics approval with study code: RAD-2559-03998/ Research ID: 3998 from Research Ethics Committee. The prospective data from five nasopharyngeal carcinoma patients who were treated using a helical tomotherapy treatment machine were used. All patients underwent intensity modulated radiotherapy (IMRT) with a plan dose of 70 Gy delivered in 33 daily fractions. Patient positioning was assured by appropriate headrest and a personalized head, neck and shoulder mask. The planning kVCT images were used in the treatment planning process. The 1<sup>st</sup> DAY MVCT images were acquired on the helical tomotherapy unit as the source images on the same day of planning kVCT image acquisitions, and the second CT scan images

were taken 20 days after starting the treatment to be the source and the target images for registration.

### 3.2.2 Images acquisitions

Regarding the kVCT images, the images were acquired on computerized tomography unit (SIEMENS Somatom, Germany) 64 slices system as in Figure 3.3(a) with the matrix of 512 x512 with 0.976 mm x 0.976 mm voxel dimension by 3 mm slice thickness.

The MVCT images were acquired on Helical Tomotherapy (Tomotherapy Inc., Madison, Wisconsin, USA) as in Figure 3.3(b). The MVCT images have a matrix of 512 x512 with 0.763 mm x 0.763 mm voxel dimension by slice thickness of 4 mm in normal scan mode.

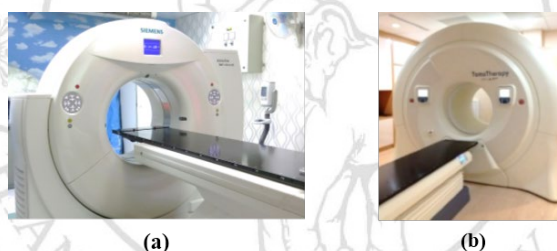


Figure 3.3 (a) Computerized tomography unit (SIEMENS Somatom, Germany) and (b) Helical Tomotherapy unit (Tomotherapy Inc., Madison, Wisconsin, USA)

### 3.2.3 Target localization

The twelve shapes of the acrylic (rigid changes) and the tissue equivalent materials (non-rigid changes) inside the cubic phantom on both kVCT and MVCT images were localized before deformation (source images) and after deformation (target images as the reference). The automatic deformed contour was assessed by comparing with the reference contour.

In the NPC cases, the region of interest (ROI) including, the target and the organ at risk (OAR) were defined by the radiation oncologist in kVCT images for treatment planning processes using Oncentra MasterPlan software version 4.3 (Nucletron, USA) as in Figure 3.4. The target, including the gross tumor volume

(GTV), is the gross demonstrated the extent and location of the tumor, the clinical target volume (CTV), is the volume of tissue that contains a demonstrable GTV and/or subclinical malignant disease with a certain probability of occurrence considered relevant for therapy. For the OARs, consist of bilateral parotid glands and spinal cord. The ROIs on the planning kVCT images were transferred to the first day MVCT images as the source images for each image set.

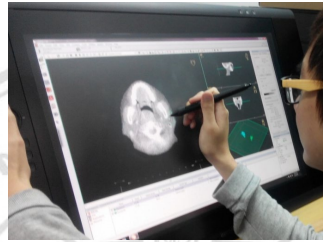


Figure 3.4 Contouring workstation (Oncentra MasterPlan, Nucletron, USA)

Regarding the DIR accuracy in unknown offset investigation, the same oncologist who localized the target and the OAR for the HT treatment planning process also contoured the GTV, CTV, both the parotid glands, and the spinal cord on the 20<sup>th</sup> kVCT images (Haksoo *et al.*, 2014; Lourenco *et al.*, 2013). Then, these were transferred to the 20<sup>th</sup> MVCT images as the reference images. These contours were compared to the automatic deformed structure generated by the deformable image registration software.

### 3.2.4 Deformable Image registration

A deformable image registration with DIRART (Figure 3.5) version 1a developed by Yang (Yang *et al.*, 2011) combined with the Computational Environment for Radiotherapy Research (CERR) version 4.6, 2013 via Matlab software were used to achieve two goals. One was to automatically create deformed contours and the other was to estimate the accumulated DVHs of the region of interest.

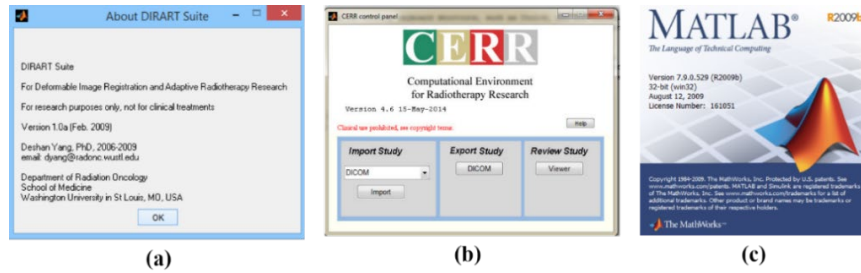


Figure 3.5 (a) DIRART software (Yang *et al.*, 2011) (b) Computational Environment for Radiotherapy Research (CERR) software version 4.6 and (c) Matlab version 7.9, 2009

The registration used the different deformation models. The eight DIR methods were performed by DIRART software with various (i) transformation frameworks (asymmetric or symmetric transformation), (ii) DIR registration algorithms (original Horn and Schunck optical flow or original Demons algorithms) and (iii) mapping direction (forward or backward mapping). The details of the DIR methods are shown in Table 3.1.

Table 3.1. Summary of all eight deformable image registration methods that varied by (i) transformation frameworks, (ii) DIR registration algorithms and (iii) mapping direction.

No.	DIR methods	Transformations		DIR Algorithms		Mapping Directions	
		Asymmetric	Symmetric	Horn & Schunck	Demons	Backward	Forward
1	Asy-HS <sub>BW</sub>	X		X		X	
2	Asy-HS <sub>FW</sub>	X		X			X
3	Asy-DM <sub>BW</sub>	X			X	X	
4	Asy-DM <sub>FW</sub>	X			X		X
5	Sym-HS <sub>BW</sub>		X	X		X	
6	Sym-HS <sub>FW</sub>		X	X			X
7	Sym-DM <sub>BW</sub>		X		X	X	
8	Sym-DM <sub>FW</sub>		X		X		X

To establish the optimum DIR performance for each algorithm, various parameters were systematically adjusted: four multigrids were used ( $n = 1, 2, 3$  and  $4$ ) with  $10n$  to  $40n$  iterations per pass (Yeo *et al.*, 2013), while the number of passes for the Horn and Schunck optical flow algorithm was 6, and the Demons algorithm

was between 2 to 6. Coarser stages were typically run with a greater number of passes to improve the agreement with the target image prior to resampling at finer resolutions (Yeo *et al.*, 2013).

### 3.2.5 Validation technique

The validation technique to compare the accuracy values of DIR between kVCT and MVCT images by different DIR methods was with respect to the intensity-based criterion, the volume-based criterion, and deformation field analysis.

Regarding the intensity-based criterion, the mean square different (MSD), the correlation coefficient (CC) and the normalized mutual information (NMI) were used to ensure image matching quality. MSD is zero when the images are correctly aligned and increases with registration error. CC can take values between -1 and +1 where +1 represents a maximum of correlation between images (Kristy *et al.*, 2013); and NMI can range between 0 and 2 and values of  $NMI > 1$  typically represent a good match between images (Penney *et al.*, 1998)

The volume-based criterion, the overlapping volume of the structure which is created by the radiation oncologist and the DIRART deformed were assessed. The most common overlap metric is the Dice Similarity Coefficient (DSC) (Kristy *et al.*, 2013). DSC is the metric that computes the number of pixels that overlap between the two volumes. If the images have no overlap, then the DSC is 0, and as the contours become identical, the DSC approaches a value close to 1 (Kristy *et al.*, 2013). Zimring *et al.* (2005) suggested that satisfactory volume matching should be 70% or more for adaptive radiotherapy application.

For deformation field analysis, the inverse consistency error (ICE) and the Jacobian analysis were used to ensure that the transformations were physically plausible. The optimal transformation was found when the ICE minimized the distance error. The Jacobian matrix describes how the transformation changes in each of the three directions. To ensure that no folding had occurred during registration, the transformation must be invertible (Lourenço *et al.*, 2013). The

Jacobian  $J_T(x) = 1$  if the volume at  $x$  remains the same after the transformation,  $J_T(x) > 1$  if there is volume expansion and  $J_T(x) < 1$  if there is volume shrinkage.

The summary of evaluation tools for each validation technique were shown in Table 3.2. The Analysis of Variance (ANOVA) with SPSS statistical software version 17 was used to compare and assess the accuracy of each DIR method.

Table 3.2 The evaluation tools in terms of the intensity-based, volume-based and deformation analysis.

Validation technique	Evaluation tools
Intensity-based	MSD, CC, NMI
Volume-based	DSC
Deformation field analysis	ICE, Jacobian analysis

### 3.3 Phase II: Accumulated dose evaluation

As regards the second research objective, the same groups of patients which used to evaluate the DIR accuracy were also used to evaluate the dosimetric impact of the deformation methods for estimating the dose accumulation on MVCT images. The first three of eight DIR methods were used to estimate the dose accumulation in this phase of the study.

#### 3.3.1 Patients

The prospective data from five nasopharyngeal carcinoma patients who treat on Helical Tomotherapy treatment machine in the Division of Therapeutic Radiology and Oncology, Faculty of Medicine, ChiangMai University were used for investigating the dose accumulation. Their tumor stages are any T or N without metastasis (M1) according to AJCC recommendation. All patients underwent Intensity Modulated Radiotherapy (IMRT) with a plan dose of 70 Gy delivered in 33 daily fractions. The patient characteristic was shown in Table 3.3.

Table 3.3 Patient characteristics.

Patient no.	Age (y)	Gender	Stage	Radiation dose/fractionation
1	55	M	T1N2M0	69.96/2.12 Gy QD
2	43	M	T4N3bM0	69.96/2.12 Gy QD
3	75	M	T4N2M0	69.96/2.12 Gy QD
4	58	F	T4N1M0	69.96/2.12 Gy QD
5	59	F	T3N1M0	69.96/2.12 Gy QD

### 3.3.2 Weekly MVCT images acquisition and target localization

When the radiotherapy treatment start, the daily MVCT images were acquired on the helical tomotherapy unit prior to each treatment fraction used for patient alignment by using a matrix of 512 x512 with voxel dimension 0.763 x 0.763 x 4 mm<sup>3</sup>. Typically the MVCT scan range covers the entire of the gross tumor volume (GTV), clinical target volume (CTV) and parotid glands bilaterally. The weekly MVCT images were used as the target images to assess the dose accumulation in this study.

Regarding the target localization, the same oncologist who localized the target and OARs for HT treatment planning process also contoured the GTV, CTV, the bilateral parotid glands, and spinal cord on the weekly MVCT images in fraction 1<sup>st</sup>, 6<sup>th</sup>, 11<sup>th</sup>, 16<sup>th</sup>, 21<sup>st</sup>, 26<sup>th</sup>, 31<sup>st</sup> as the reference images. These contours were compared to the automatic deformed structure generated by the deformable image registration software.

### 3.3.3 Treatment planning system

As regards the TomoTherapy treatment planning system, A planning station on Hi Art software, version 4.2.3 (Tomotherapy Inc., Madison, Wisconsin, USA) were used for IMRT treatment planning. The dose distribution and dose volume histogram (DVH) of each patient were evaluated by the radiation oncologist for the IMRT treatment delivery on the helical tomotherapy unit.

Regarding the dose accumulation, to ensure the accuracy of dose accumulation which estimated on DIRART and CERR software, the Plan Adaptive (Hi Art software v.4.2.3, Tomotherapy Inc., Wisconsin, USA), the independent software was used to compare the weekly dose accumulation. The treatment planning systems are shown in Figure 3.6.



Figure 3.6 Tomotherapy Treatment Planning (Tomotherapy, WI, USA) (a) Planning station software (b) Planned Adaptive software and (c) dose distribution.

### 3.3.4 Dose accumulation and dose comparison

Regarding the second objective of this study, the dosimetric impact of the deformation methods for estimating the dose accumulation on MVCT images were evaluated. Therefore, this context aimed to calculate the weekly and cumulative dose distributions received by the patient while accounting for anatomic variations.

The dose accumulation process relied on the six steps, as illustrated in Figure 3.7. Firstly, the ROIs from planning kVCT images were transferred to the 1<sup>st</sup> DAY MVCT as the source images for registration. The top three DIR methods which received from phase I were performed between the 1<sup>st</sup> DAY MVCT and the weekly MVCTs (step 2). Applied the deformation vector field for created the automatic deformed the ROIs and propagation to the weekly MVCT images (step 3) and deformed the weekly dose distribution (step 4). The weekly dose deformation was summed to the accumulated dose (step 5) and compared to the initial planning dose distribution (step 6). The dose distributions were accumulated and displayed on CERR software via Matlab.

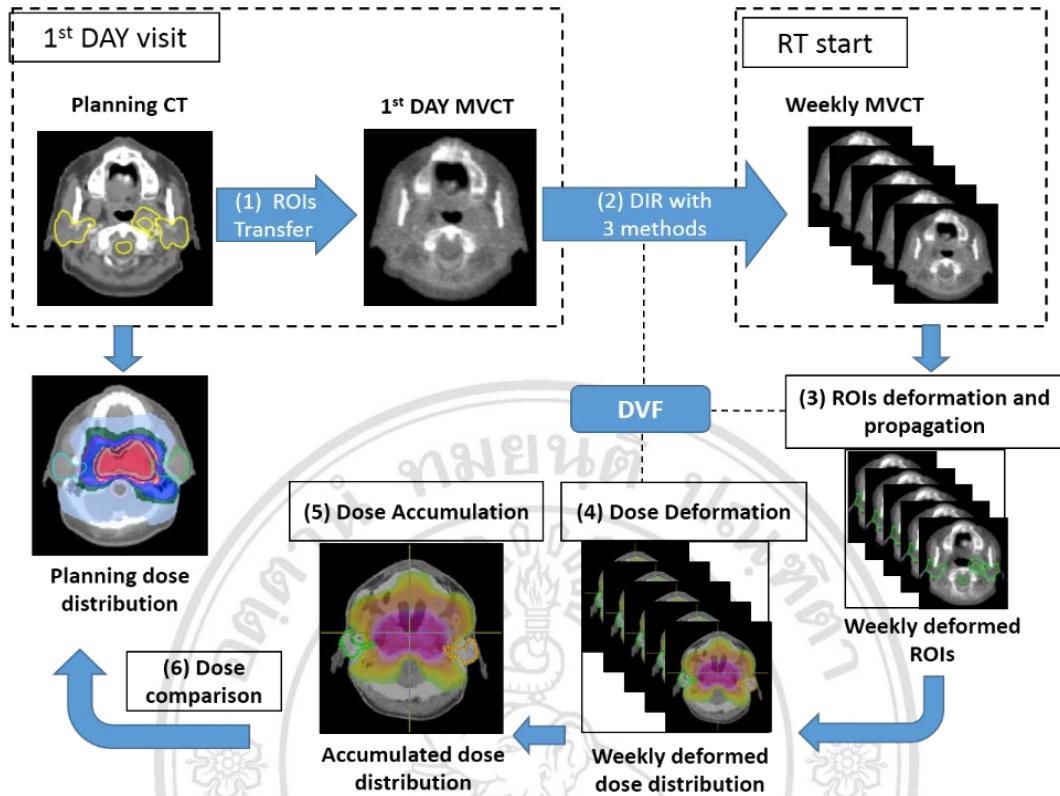


Figure 3.7 The diagram of study workflow for dose accumulation and dose comparison

As regards the accumulated dose comparison, for the target volume, the median absorbed dose ( $D_{50\%}$ ), near-minimum absorbed dose ( $D_{98\%}$ ) and near-maximum absorbed dose ( $D_{2\%}$ ) values from each DIR method were assessed,  $D_{\text{mean}}$ ,  $D_{50\%}$  of bilateral parotid glands and  $D_{2\%}$  of spinal cord were compared to the original planned dose for the OARs investigation as the detail in Table 3.4 (Lourenço *et al.*, 2013; Stuart *et al.*, 2010). A one-way ANOVA test and paired sample t-test were carried out on each set of comparison metric to determine statistical significance, with a threshold of  $p < 0.05$  with SPSS statistical software version 17 were used to compare and assess the impact of each of the DIR methods.

Table 3.4 The dose reporting for each ROIs to the comparison of accumulated dose and initial planned dose.

ROIs	Dose reporting (Gy)
GTV	D <sub>50%</sub> , D <sub>2%</sub> , D <sub>98%</sub>
CTV	D <sub>50%</sub> , D <sub>2%</sub> , D <sub>98%</sub>
Bilateral parotid gland	D <sub>mean</sub> , D <sub>50%</sub>
Spinal cord	D <sub>2%</sub>



ลิขสิทธิ์มหาวิทยาลัยเชียงใหม่  
 Copyright© by Chiang Mai University  
 All rights reserved